A Unified Approach to the Design of PWM-Based Sliding-Mode Voltage Controllers for Basic DC-DC Converters in Continuous Conduction Mode

Siew-Chong Tan, *Member, IEEE*, Y. M. Lai, *Member, IEEE*, and Chi K. Tse, *Fellow, IEEE*

***Abstract*—This paper presents a simple unified approach to the design of fixed-frequency pulsewidth-modulation-based sliding-mode controllers for dc–dc converters operating in the continuous conduction mode. The design methodology is illustrated on the three primary dc–dc converters: buck, boost, and buck–boost converters. To illustrate the feasibility of the scheme, an experimental prototype of the derived boost controller/converter system is developed. Several tests are performed to validate the functionalities of the system.**

***Index Terms*—Continuous conduction mode (CCM), dc–dc converter, nonlinear controller, pulsewidth modulation (PWM), sliding-mode (SM) control.**

I. Introduction

SLIDING-MODE (SM) controllers are well known for their robustness and stability. Ideally, SM controllers operate at infinite, varying, and self-oscillating switching frequency such that the controlled variables can track a certain reference path to achieve the desired steady-state operation [1]. However, due to the varying and high switching frequency, the feasibility of applying SM controllers in power converters is challenged. First, extreme high-speed switching operation in power converters results in excessive switching losses, inductor and transformer core losses, and electromagnetic interference (EMI) issues. Second, variable switching frequency complicates the design of the input and output filters [2]. Hence, for SM controllers to be truly applicable to power converters, their switching frequencies must be constricted within a practical range.

Numerous methods have been proposed to constrict the switching frequency of SM controllers [3]–[11]. In particular, those employing the hysteresis-modulation (HM) (or delta-modulation) for implementing the control law normally require either constant timer circuits to be incorporated to ensure constant switching frequency operation [3], [4], or the use of an adaptive hysteresis band that varies with parameter changes to limit the variation of the switching frequency [5]. However, these solutions require additional components and are unattractive for low cost voltage conversion applications. Furthermore, due to the imposition of the ramp or timing function onto the SM switching function, the resulting converter system may suffer from deteriorated transient response.

Manuscript received January 11, 2005; revised June 23, 2005, September 6, 2005, November 21, 2005, and February 26, 2006. This paper was recommended by Associate Editor M. Kazimierczuk.

The authors are with the Department of Electronic and Information Engineering, The Hong Kong Polytechnic University, Hong Kong (e-mail: ensctan@eie.polyu.edu.hk).

Digital Object Identifier 10.1109/TCSI.2006.879052

Alternatively, the variation of the switching frequency of SM controllers can be limited by changing the modulation method of the SM controllers from HM to pulsewidth modulation (PWM), which is sometimes known as the duty cycle control [6]–[9], [11], [12]. This idea can be rooted back to one of the earliest papers on SM controlled power converters [12], which suggested that under SM control operation, the control signal of an *equivalent control approach* $u_{\rm eq}$ in SM control is equivalent to the *duty cycle control signal* D of a PWM controller. Later, Sira-Ramirez *et al.* [13] proposed a geometric framework to map the PWM feedback control onto SM control and provided a rigorous proof of the equivalence between SM and PWM controllers [14]. It has been shown that as the switching frequency tends to infinity, the averaged dynamics of a SM controlled system is equivalent to the averaged dynamics of a PWM controlled system, thus establishing the relationship $u_{\rm eq} = d$. On the other hand, the same correlation has been derived in Martinez *et al.* [15], where the nonlinear PWM continuous control was compared with an equivalent control. In their method, an average representation of the converter model was employed. Hence, the migration of a SM controller from being HM based to PWM based is made possible. Unfortunately, the theory was not exploited to initiate the development of such controllers.

The first useful clue to how PWM techniques can be applied to SM control to develop fixed-frequency SM controllers is probably due to Nguyen and Lee [7]. In two other related papers [8] and [9], the *state-space averaging technique* is incorporated into the controller's modeling. By doing so, PWM duty cycle control can be directly applied to the implementation of SM controllers. This method of large signal averaging was also adopted in [16], which implemented a PWM-based second-order SM controller on a buck converter. However, while these papers provided encouraging evidence on the feasibility of developing such SM controllers, they fall short of a detailed study of the technical aspects of the implementation. It is only recently that the idea is revisited and experimentally demonstrated on a SM voltage controlled (SMVC) buck converter [11]. Building on the work of [7], [12]–[14], we demonstrate in [11] how PWM-based SM controllers can be easily realized with simple analog integrated circuits (ICs). Additionally, the earlier work [11] has also presented the design methodology from a simple circuit design perspective so that it can be conveniently adopted by practising engineers.

Hence, in this paper, we develop a unified approach based on the work of [11], to the design of PWM-based SM voltage controllers for all basic dc–dc converter types. Similar to [11], our aim is to present simple and ready-to-use control equations for immediate implementation of the PWM-based SM voltage

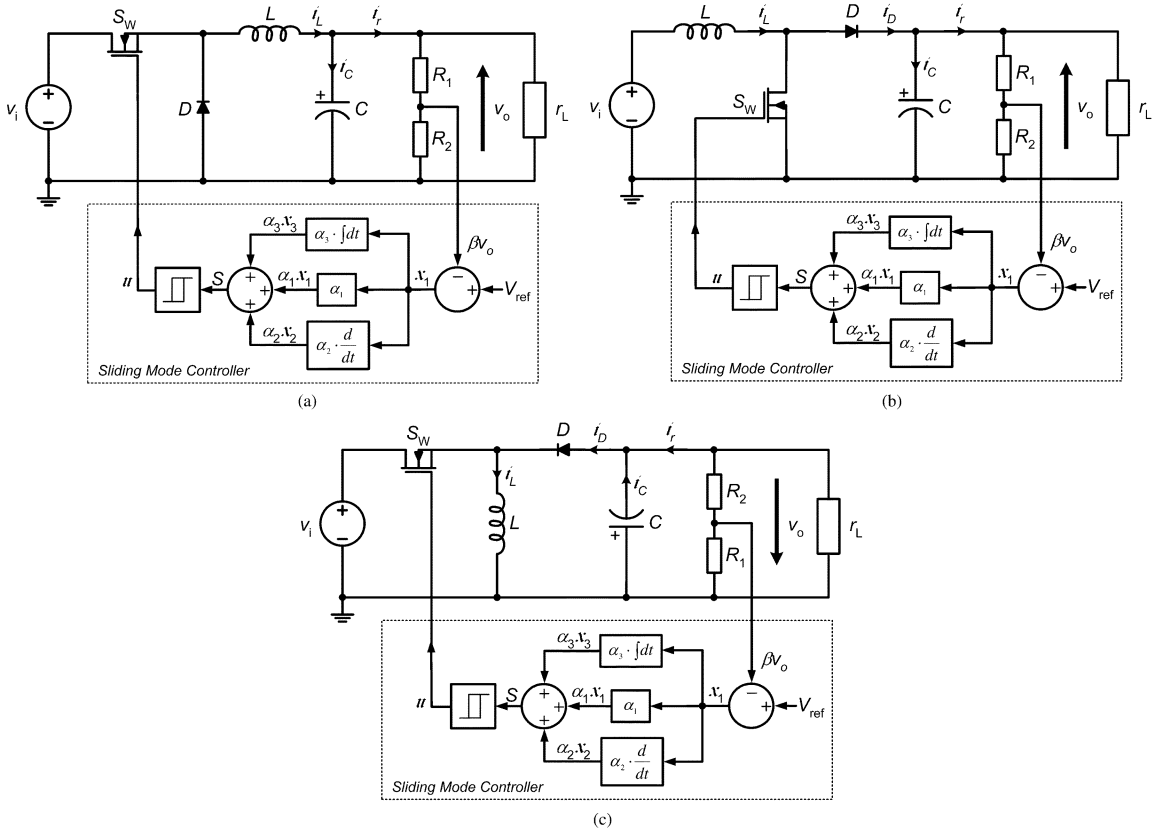

Fig. 1. Schematic diagrams of conventional HM-based PID SMVC converteres. (a) SMVC buck converter. (b) SMVC boost converter. (c) SMVC bulk-boost converter.

controller. It is also worth mentioning that even though the discussion covers only the buck, boost, and buck–boost converters, the approach is applicable to all other dc–dc converter types.

II. Approach

The detailed discussion of SM control theory, equivalent control method, and the relationship of SM control and duty ratio control, can be found in [1], [13], and [14]. In the following, we outline the modeling method and describe the detailed procedures for designing SM controllers for dc–dc converters in continuous conduction mode (CCM) operation.

A. System Modeling

The first step to the design of an SM controller is to develop a state-space description of the converter model in terms of the desired control variables (i.e., voltage and/or current etc,). Our focus in this paper is the application of SM control to converters operating in CCM. The controller under study is a second-order proportional integral derivative (PID) SM voltage controller. Unlike most previously proposed SM voltage controllers, it takes into account an additional voltage error integral term in the control computation to reduce the steady-state dc error of the practical SM controlled system.

Fig. 1 shows the schematic diagrams of the three PID SMVC dc–dc converters to be discussed in this paper in the conventional HM configuration. Here, C, L, and r_L denote the capacitance, inductance, and instantaneous load resistance of the converters respectively; i_C, i_L, and i_r denote the instantaneous capacitor, inductor, and load currents, respectively; $V_{\rm ref}, v_i$, and v_o denote the reference, instantaneous input, and instantaneous output voltages, respectively; β denotes the feedback network ratio; and $u = 0$ or 1 is the switching state of power switch S_W.

In the case of PID SMVC converters, the control variable $\boldsymbol{x}$ may be expressed in the following form:

$$\boldsymbol{x} = \begin{bmatrix} x_1 \\ x_2 \\ x_3 \end{bmatrix} = \begin{bmatrix} V_{\rm ref} - \beta v_o \\ \frac{d(V_{\rm ref} - \beta v_o)}{dt} \\ \int (V_{\rm ref} - \beta v_o) dt \end{bmatrix} \tag{1}$$

where x_1, x_2, and x_3 are the *voltage error*, the *voltage error dynamics* (or the rate of change of voltage error), and the *integral of voltage error*, respectively.

Substitution of the converters' behavioral models under CCM into (1) produces the following control variable descriptions: $\boldsymbol{x}_{\rm buck}, \boldsymbol{x}_{\rm boost}$, and $\boldsymbol{x}_{\rm buck-boost}$ for buck, boost, and buck–boost converter, respectively

$$\boldsymbol{x}_{\rm buck} = \begin{bmatrix} x_1 = V_{\rm ref} - \beta v_o \\ x_2 = \frac{\beta v_o}{r_L C} + \int \frac{\beta(v_o - v_i u)}{LC} dt \\ x_3 = \int x_1 dt \end{bmatrix} \tag{2}$$

$$\boldsymbol{x}_{\rm boost} = \begin{bmatrix} x_1 = V_{\rm ref} - \beta v_o \\ x_2 = \frac{\beta v_o}{r_L C} + \int \frac{\beta(v_o - v_i)\bar{u}}{LC} dt \\ x_3 = \int x_1 dt \end{bmatrix} \tag{3}$$

$$\boldsymbol{x}_{\rm buck-boost} = \begin{bmatrix} x_1 = V_{\rm ref} - \beta v_o \\ x_2 = \frac{\beta v_o}{r_L C} + \int \frac{\beta v_o \bar{u}}{LC} dt \\ x_3 = \int x_1 dt \end{bmatrix}. \tag{4}$$

TABLE I
MATRIX DESCRIPTIONS OF SMVC BUCK, BOOST, AND BUCK–BOOST CONVERTERS OPERATING IN CCM

Type of Converter	**A**	**B**	**D**	v
Buck	$\begin{bmatrix} 0 & 1 & 0 \\ 0 & -\frac{1}{r_L C} & 0 \\ 1 & 0 & 0 \end{bmatrix}$	$\begin{bmatrix} 0 \\ -\frac{\beta v_i}{LC} \\ 0 \end{bmatrix}$	$\begin{bmatrix} 0 \\ \frac{\beta v_o}{LC} \\ 0 \end{bmatrix}$	u
Boost	$\begin{bmatrix} 0 & 1 & 0 \\ 0 & -\frac{1}{r_L C} & 0 \\ 1 & 0 & 0 \end{bmatrix}$	$\begin{bmatrix} 0 \\ \frac{\beta v_o}{LC} - \frac{\beta v_i}{LC} \\ 0 \end{bmatrix}$	$\begin{bmatrix} 0 \\ 0 \\ 0 \end{bmatrix}$	$\bar{u}$
Buck-boost	$\begin{bmatrix} 0 & 1 & 0 \\ 0 & -\frac{1}{r_L C} & 0 \\ 1 & 0 & 0 \end{bmatrix}$	$\begin{bmatrix} 0 \\ \frac{\beta v_o}{LC} \\ 0 \end{bmatrix}$	$\begin{bmatrix} 0 \\ 0 \\ 0 \end{bmatrix}$	$\bar{u}$

Next, the time differentiation of (2), (3), and (4) produces the state-space descriptions required for the controller design of the respective converter.

For the buck converter

$$\begin{bmatrix} \dot{x_1} \\ \dot{x_2} \\ \dot{x_3} \end{bmatrix} = \begin{bmatrix} 0 & 1 & 0 \\ 0 & -\frac{1}{r_L C} & 0 \\ 1 & 0 & 0 \end{bmatrix} \begin{bmatrix} x_1 \\ x_2 \\ x_3 \end{bmatrix} + \begin{bmatrix} 0 \\ -\frac{\beta v_i}{LC} \\ 0 \end{bmatrix} u + \begin{bmatrix} 0 \\ \frac{\beta v_o}{LC} \\ 0 \end{bmatrix}. \quad (5)$$

For the boost converter

$$\begin{bmatrix} \dot{x_1} \\ \dot{x_2} \\ \dot{x_3} \end{bmatrix} = \begin{bmatrix} 0 & 1 & 0 \\ 0 & -\frac{1}{r_L C} & 0 \\ 1 & 0 & 0 \end{bmatrix} \begin{bmatrix} x_1 \\ x_2 \\ x_3 \end{bmatrix} + \begin{bmatrix} 0 \\ \frac{\beta v_o}{LC} - \frac{\beta v_i}{LC} \\ 0 \end{bmatrix} \bar{u}. \quad (6)$$

For the buck–boost converter

$$\begin{bmatrix} \dot{x_1} \\ \dot{x_2} \\ \dot{x_3} \end{bmatrix} = \begin{bmatrix} 0 & 1 & 0 \\ 0 & -\frac{1}{r_L C} & 0 \\ 1 & 0 & 0 \end{bmatrix} \begin{bmatrix} x_1 \\ x_2 \\ x_3 \end{bmatrix} + \begin{bmatrix} 0 \\ \frac{\beta v_o}{LC} \\ 0 \end{bmatrix} \bar{u} \quad (7)$$

where $\bar{u} = 1 - u$ is the inverse logic of u, used particularly for modeling the boost and buck–boost topologies. Rearrangement of the state-space descriptions (5), (6), and (7) into the standard form gives

$$\dot{\boldsymbol{x}} = \mathbf{A}\boldsymbol{x} + \mathbf{B}v + \mathbf{D} \quad (8)$$

where $v = u$ or $\bar{u}$ (depending on topology). Results are summarized in the tabulated format shown in Table I.

B. Controller Design

Having obtained the state-space descriptions, the next stage is the design of the controller. For these systems, it is appropriate to have a general SM control law that adopts a switching function such as

$$u = \begin{cases} 1, & \text{when } S > 0 \\ 0, & \text{when } S < 0 \end{cases} \quad (9)$$

where S is the instantaneous state variable's trajectory, and is described as

$$S = \alpha_1 x_1 + \alpha_2 x_2 + \alpha_3 x_3 = \boldsymbol{J}^{\mathbf{T}}\boldsymbol{x} \quad (10)$$

with $\boldsymbol{J}^{\mathbf{T}} = [\alpha_1\ \alpha_2\ \alpha_3]$ and α_1, α_2, and α_3 representing the control parameters termed as sliding coefficients.

1) Derivation of Existence Conditions: Next, we consider how the existence conditions[1] of SM control operation are obtained for the converters. To ensure the existence of SM operation, the local reachability condition

$$\lim_{S \to 0} S \cdot \dot{S} < 0 \quad (11)$$

must be satisfied. This can be expressed as

$$\begin{cases} \dot{S}_{S \to 0^+} = \boldsymbol{J}^{\mathbf{T}}\mathbf{A}\boldsymbol{x} + \boldsymbol{J}^{\mathbf{T}}\mathbf{B}v_{S \to 0^+} + \boldsymbol{J}^{\mathbf{T}}\mathbf{D} < 0 \\ \dot{S}_{S \to 0^-} = \boldsymbol{J}^{\mathbf{T}}\mathbf{A}\boldsymbol{x} + \boldsymbol{J}^{\mathbf{T}}\mathbf{B}v_{S \to 0^-} + \boldsymbol{J}^{\mathbf{T}}\mathbf{D} > 0. \end{cases} \quad (12)$$

Example—Buck Converter:

- Case 1: $S \to 0^+, \dot{S} < 0$:
  Substitution of $v_{S \to 0^+} = u = 1$ and the matrices in Table I into (12) gives

$$-\alpha_1 \frac{\beta i_C}{C} + \alpha_2 \frac{\beta i_C}{r_L C^2} + \alpha_3 (V_{\text{ref}} - \beta v_o) - \alpha_2 \frac{\beta v_i}{LC} + \alpha_2 \frac{\beta v_o}{LC} < 0. \quad (13)$$

- Case 2: $S \to 0^-, \dot{S} > 0$:
  Substitution of $v_{S \to 0^-} = u = 0$ and the matrices in Table I into (12) gives

$$-\alpha_1 \frac{\beta i_C}{C} + \alpha_2 \frac{\beta i_C}{r_L C^2} + \alpha_3 (V_{\text{ref}} - \beta v_o) + \alpha_2 \frac{\beta v_o}{LC} > 0. \quad (14)$$

  Finally, the combination of (13) and (14) gives the simplified existence condition

$$0 < -\beta L \left(\frac{\alpha_1}{\alpha_2} - \frac{1}{r_L C} \right) i_C + LC \frac{\alpha_3}{\alpha_2} (V_{\text{ref}} - \beta v_o) + \beta v_o < \beta v_i. \quad (15)$$

Example—Boost Converter:

- Case 1: $S \to 0^+, \dot{S} < 0$:
  Substitution of $v_{S \to 0^+} = \bar{u} = 0$ and the matrices in Table I into (12) gives

$$-\alpha_1 \frac{\beta i_C}{C} + \alpha_2 \frac{\beta i_C}{r_L C^2} + \alpha_3 (V_{\text{ref}} - \beta v_o) < 0. \quad (16)$$

[1]Satisfaction of the existence conditions is one of the three necessary requirements for SM control operation to occur. It ensures that the trajectory at locations near the sliding surface will always be directed towards the sliding surface. The other two necessary requirements are the hitting condition, which is satisfied by the control law in (9), and the stability condition, which is satisfied through the assignment of sliding coefficients [17].

TABLE II
EXISTENCE CONDITIONS OF BUCK, BOOST, AND BUCK–BOOST CONVERTERS OPERATING IN CCM

Buck	$0 < -\beta L\left(\frac{\alpha_1}{\alpha_2} - \frac{1}{r_{\mathrm{L(min)}}C}\right) i_{C(\mathrm{SS})} + LC\frac{\alpha_3}{\alpha_2}\left(V_{\mathrm{ref}} - \beta v_{\mathrm{o(SS)}}\right) + \beta v_{\mathrm{o(SS)}} < \beta v_{\mathrm{i(min)}}$
Boost	$0 < \beta L\left(\frac{\alpha_1}{\alpha_2} - \frac{1}{r_{\mathrm{L(min)}}C}\right) i_{C(\mathrm{SS})} - LC\frac{\alpha_3}{\alpha_2}\left(V_{\mathrm{ref}} - \beta v_{\mathrm{o(SS)}}\right) < \beta(v_{\mathrm{o(SS)}} - v_{\mathrm{i(max)}})$
Buck-boost	$0 < \beta L\left(\frac{\alpha_1}{\alpha_2} - \frac{1}{r_{\mathrm{L(min)}}C}\right) i_{C(\mathrm{SS})} - LC\frac{\alpha_3}{\alpha_2}\left(V_{\mathrm{ref}} - \beta v_{\mathrm{o(SS)}}\right) < \beta v_{\mathrm{o(SS)}}$

- Case 2: $S \to 0^-, \dot{S} > 0$:
  Substitution of $v_{S\to 0^-} = \bar{u} = 1$ and the matrices in Table I into (12) gives

$$-\alpha_1\frac{\beta i_C}{C} + \alpha_2\frac{\beta i_C}{r_L C^2} + \alpha_3(V_{\mathrm{ref}} - \beta v_o) - \alpha_2\frac{\beta v_i}{LC} + \alpha_2\frac{\beta v_o}{LC} > 0. \tag{17}$$

  Finally, the combination of (16) and (17) gives the simplified existence condition

$$0 < \beta L\left(\frac{\alpha_1}{\alpha_2} - \frac{1}{r_L C}\right) i_C - LC\frac{\alpha_3}{\alpha_2}(V_{\mathrm{ref}} - \beta v_o) < \beta(v_o - v_i). \tag{18}$$

The derived existence conditions for the buck, boost, and buck–boost[2] converters are tabulated in Table II. The selection of sliding coefficients for the controller of each converter must comply to its stated inequalities. We have taken into account the complete ranges of operating conditions (minimum and maximum input voltages, i.e., $v_{i(\min)}$ and $v_{i(\max)}$, and minimum and maximum load resistances, i.e., $r_{L(\min)}$ and $r_{L(\max)}$). This assures the compliance of the existence condition for the full operating ranges of the converters.

Additionally, it should be noted that the inequalities involve not only the system parameters and the sliding coefficients, but also the various instantaneous state variables of the system, which complicates the evaluation. In the case of designing an SM controller with a static sliding surface, a practical approach is to design the sliding coefficients to meet the existence conditions for steady-state operations [11], [18]–[20]. Under such consideration, the state variables i_C and v_o can be substituted with their expected steady-state parameters, i.e., $i_{C(\mathrm{SS})}$ and $v_{o(\mathrm{SS})}$, which can be derived from the design specification. This assures the compliance of the existence condition at least in the small region of the origin.

Finally, in converters with high system parameters uncertainty, it is necessary to also consider the circuit component tolerances when evaluating the inequalities.

2) Selection of Sliding Coefficients: Clearly, the inequalities in Table II provide only the general information for the existence of SM, but give no details about the selection of the parameters. For this purpose, we employ the Ackermann's Formula for designing static controllers [17]. This basically concerns with the selection of sliding coefficients based on the desired dynamic properties. In this way, the *stability condition*[3] of the system is automatically satisfied. This is a direct approach of assuring stability, whereby the same objective of making the *eigenvalues* of the *Jacobian matrix* of the system in SM operation to contain negative real parts is achieved.

In our example, the equation relating the sliding coefficients to the dynamic response of the converter during SM operation can be easily found by solving $S = 0$, which results in a linear second-order equation with three possible types of responses: under-damped ($0 \le \zeta < 1$), critically damped ($\zeta = 1$), and over-damped ($\zeta > 1$).

In the case of under-damped response converters, the desired settling time $T_s = 5\tau$ s (1% criteria), where τ is the natural time constant, can be set by tuning (α_1/α_2) using

$$\frac{\alpha_1}{\alpha_2} = \frac{10}{T_s} \tag{19}$$

and the desired damping ratio can be set using

$$\frac{\alpha_3}{\alpha_2} = \frac{25}{\zeta^2 {T_s}^2} \tag{20}$$

where

$$\zeta = \sqrt{\frac{\left[\ln\left(\frac{M_p}{100}\right)\right]^2}{\pi^2 + \left[\ln\left(\frac{M_p}{100}\right)\right]^2}} \tag{21}$$

where M_p is the percentage of the peak overshoot.

Note that the 5τ s (1% criteria) settling time assumed in the derivation is the time taken for the controller to complete the *SM operation phase*, i.e., the time taken for the state variable trajectory S to track from any point on the sliding surface to the steady-state equilibrium. This time period does not include the *reaching phase*, which itself requires a relatively small, but finite time period for S to move from an arbitrary position (depending on the magnitude of the load or line disturbance and the capacity of the energy storage element) to the sliding surface. Theoretically, the total time taken to complete both the SM operation phase and the reaching phase is equivalent to the settling time T_s for the converter. However, in practice, considering that the

[2]The derivation procedure of the existence condition for the buck–boost converter is similar to that of the boost converter.

[3]Satisfaction of the stability condition ensures that the state trajectory of the system under SM operation will always reach a stable equilibrium point.

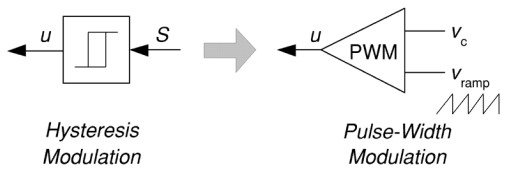

Fig. 2. Basic structure of hysteresis modulator and pulsewidth modulator.

time taken to complete the SM operation phase is usually much greater than the reaching phase, it is sufficient to consider only the SM operation phase time as the settling time. Furthermore, it should also be clarified that the aforementioned settling time description is only strictly true for an ideal SM controller with infinite switching frequency. For a finite-switching-frequency SM controller, i.e., PWM-based SM controller, the settling time will be slightly longer than the ideal case due to the nonideality of the tracking motion.

Thus, the design of the sliding coefficients is now dependent on the desired settling time of the response and the type and amount of damping required, in conjunction with the existence condition of the respective PWM-based controllers. It is worth mentioning that the design equations in (19) and (20) are applicable to all types of dc–dc converters.

3) Derivation of Control Equations for PWM-Based Controller: The conventional SM controller implementation based on HM [10] requires only control (9) and (10). The same controller is used for all three converters. However, if the PWM-based SM voltage controller is to be adopted [11], an indirect translation of the SM control law is required so that PWM can be used in lieu of hysteretic modulation (see Fig. 2). This results in a unique controller for each converter since their control equations are all different. A detailed description of this implementation for the buck converter is provided in [11]. It can be summarized in two steps. Firstly, the equivalent control signal $u_{\rm eq}$, which is a smooth function of the discrete input function u, is formulated using the *invariance conditions* by setting the time differentiation of (10) as $\dot{S} = 0$ [1]. Secondly, the equivalent control function is mapped onto the instantaneous duty cycle function d of the pulsewidth modulator [11].

Example—Buck Converter: Equating $\dot{S} = \boldsymbol{J}^{\mathbf{T}}\mathbf{A}\boldsymbol{x} + \boldsymbol{J}^{\mathbf{T}}\mathbf{B}u_{\rm eq} + \boldsymbol{J}^{\mathbf{T}}\mathbf{D} = 0$ yields the equivalent control function

$$\begin{aligned} u_{\rm eq} &= -[\boldsymbol{J}^{\mathbf{T}}\mathbf{B}]^{-1}\boldsymbol{J}^{\mathbf{T}}[\mathbf{A}\boldsymbol{x}+\mathbf{D}] \\ &= -\frac{\beta L}{\beta v_i}\left(\frac{\alpha_1}{\alpha_2}-\frac{1}{r_L C}\right) i_C \\ &\quad + \frac{\alpha_3 LC}{\alpha_2 \beta v_i}(V_{\rm ref}-\beta v_o) + \frac{v_o}{v_i} \end{aligned} \tag{22}$$

where $u_{\rm eq}$ is continuous and $0 < u_{\rm eq} < 1$. Substitution of (22) into the inequality gives

$$\begin{aligned} 0 < u_{\rm eq} = -\frac{\beta L}{\beta v_i}\left(\frac{\alpha_1}{\alpha_2}-\frac{1}{r_L C}\right) i_C \\ + \frac{\alpha_3 LC}{\alpha_2 \beta v_i}(V_{\rm ref}-\beta v_o) + \frac{v_o}{v_i} < 1. \end{aligned}$$

Multiplication of the inequality by βv_i gives

$$\begin{aligned} 0 < {u_{\rm eq}}^* = -\beta L\left(\frac{\alpha_1}{\alpha_2}-\frac{1}{r_L C}\right) i_C \\ + LC\frac{\alpha_3}{\alpha_2}(V_{\rm ref}-\beta v_o) + \beta v_o < \beta v_i. \end{aligned} \tag{23}$$

Finally, the mapping of the equivalent control function (23) onto the duty ratio control d, where $0 < d = (v_c/\hat{v}_{\rm ramp}) < 1$, gives the following relationships for the control signal v_c and ramp signal $\hat{v}_{\rm ramp}$ for the practical implementation of the PWM-based SM controller

$$\begin{aligned} v_c = {u_{\rm eq}}^* = -\beta L\left(\frac{\alpha_1}{\alpha_2}-\frac{1}{r_L C}\right) i_C \\ + \frac{\alpha_3}{\alpha_2} LC(V_{\rm ref}-\beta v_o) + \beta v_o \end{aligned} \tag{24}$$

and

$$\hat{v}_{\rm ramp} = \beta v_i. \tag{25}$$

Example—Boost Converter: Equating $\dot{S} = \boldsymbol{J}^{\mathbf{T}}\mathbf{A}\boldsymbol{x} + \boldsymbol{J}^{\mathbf{T}}\mathbf{B}\bar{u}_{\rm eq} = 0$ yields the equivalent control function

$$\begin{aligned} \bar{u}_{\rm eq} &= -[\boldsymbol{J}^{\mathbf{T}}\mathbf{B}]^{-1}\boldsymbol{J}^{\mathbf{T}}\mathbf{A}\boldsymbol{x} \\ &= \frac{\beta L}{\beta\,(v_o - v_i)}\left(\frac{\alpha_1}{\alpha_2}-\frac{1}{r_L C}\right) i_C \\ &\quad - \frac{\alpha_3 LC}{\alpha_2 \beta\,(v_o - v_i)}(V_{\rm ref}-\beta v_o) \end{aligned} \tag{26}$$

where $\bar{u}_{\rm eq}$ is continuous and $0 < \bar{u}_{\rm eq} < 1$. Substitution of (26) into the inequality gives

$$\begin{aligned} 0 < \bar{u}_{\rm eq} = \frac{\beta L}{\beta(v_o - v_i)}\left(\frac{\alpha_1}{\alpha_2}-\frac{1}{r_L C}\right) i_C \\ - \frac{\alpha_3 LC}{\alpha_2 \beta(v_o - v_i)}(V_{\rm ref}-\beta v_o) < 1. \end{aligned}$$

Since $u = 1 - \bar{u}$, which also implies $u_{\rm eq} = 1 - \bar{u}_{\rm eq}$, the inequality can be rewritten as

$$\begin{aligned} 0 < u_{\rm eq} = 1 - \left[\frac{\beta L}{\beta(v_o - v_i)}\left(\frac{\alpha_1}{\alpha_2}-\frac{1}{r_L C}\right) i_C \right. \\ \left. - \frac{\alpha_3 LC}{\alpha_2 \beta(v_o - v_i)}(V_{\rm ref}-\beta v_o)\right] < 1. \end{aligned}$$

Multiplication of the inequality by $\beta(v_o - v_i)$ gives

$$\begin{aligned} 0 < {u_{\rm eq}}^* = -\beta L\left(\frac{\alpha_1}{\alpha_2}-\frac{1}{r_L C}\right) i_C + LC\frac{\alpha_3}{\alpha_2}(V_{\rm ref} \\ -\beta v_o) + \beta(v_o - v_i) < \beta(v_o - v_i). \end{aligned} \tag{27}$$

Finally, the mapping of the equivalent control function (27) onto the duty ratio control d, where $0 < d = (v_c)/(\hat{v}_{\rm ramp}) < 1$, gives the following relationships for the control signal v_c and ramp signal $\hat{v}_{\rm ramp}$ for the practical implementation of the PWM-based SM controller

$$\begin{aligned} v_c &= {u_{\rm eq}}^* \\ &= -\beta L\left(\frac{\alpha_1}{\alpha_2}-\frac{1}{r_L C}\right) i_C + LC\frac{\alpha_3}{\alpha_2}(V_{\rm ref}-\beta v_o) \\ &\quad + \beta(v_o - v_i) \end{aligned} \tag{28}$$

and

$$\hat{v}_{\rm ramp} = \beta(v_o - v_i). \tag{29}$$

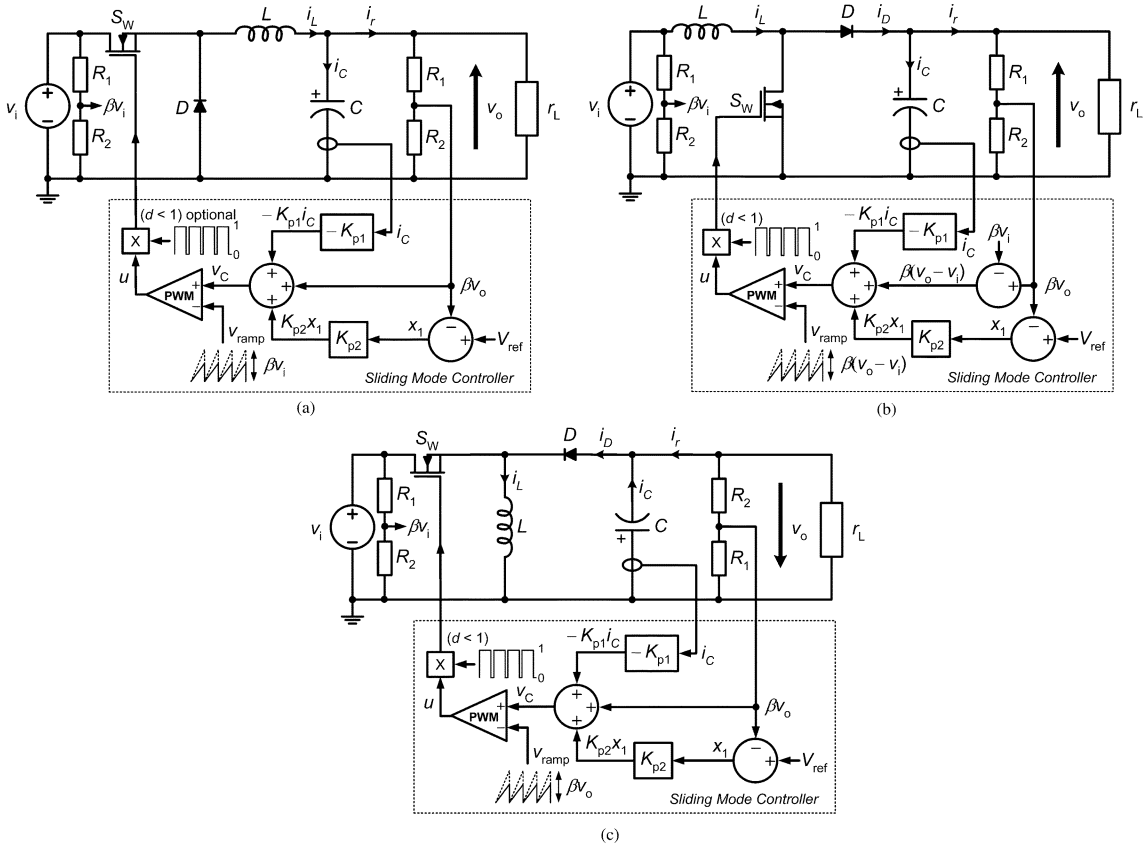

Fig. 3. Schematic diagrams of the PWM-based PID SMVC converters. (a) SMVC buck converter. (b) SMVC boost converter. (c) SMVC bulk-boost converter.

The control equations required for the implementation of the respective buck, boost, and buck–boost[4] PWM-based SMVC converters are tabulated in Table III. K_{p1} and K_{p2} are the constant gain parameters for the feedback signals i_C and $(V_{\text{ref}} - \beta v_o)$. The values of K_{p1} and K_{p2} can be found in terms of converter's parameters L, C, and r_L, and values of sliding coefficients α_1, α_2, and α_3, which must comply with the existence condition shown in Table II.

TABLE III
CONTROL EQUATIONS OF PWM-BASED SMVC BUCK, BOOST, AND BUCK–BOOST CONVERTERS OPERATING IN CCM

Type of Converter	v_c	$\hat{v}_{\text{ramp}}$
Buck	$-K_{p1} i_C + K_{p2}(V_{\text{ref}} - \beta v_o) + \beta v_o$	βv_i
Boost	$-K_{p1} i_C + K_{p2}(V_{\text{ref}} - \beta v_o) + \beta(v_o - v_i)$	$\beta(v_o - v_i)$
Buck-boost	$-K_{p1} i_C + K_{p2}(V_{\text{ref}} - \beta v_o) + \beta v_o$	βv_o

* K_{p1} and K_{p2} are parameters calculated using $K_{p1} = \beta L\left(\frac{\alpha_1}{\alpha_2} - \frac{1}{r_L C}\right)$ and $K_{p2} = \frac{\alpha_3}{\alpha_2} LC$.

C. Remarks

1) Controller Structure: Fig. 3 shows the schematic diagrams of the respective PWM-based SMVC converters. The controller designs are based on the equations illustrated in Table III. Careful examination of these circuits reveal that they basically adopts the same structure as the PWM PD linear control, but with additional components consisting of the instantaneous input voltage βv_i and/or the instantaneous output voltage βv_o. These are the components contributing to the nonlinearity of the feedback control, and are therefore the key properties keeping the controller robust to load and line regulation under wide operating ranges. It should also be noted that the integral term of the control variable, i.e., x_3, is implicitly hidden in the control variable v_o. In case of large disturbance, this component is highly influential in the control. However, when the steady state is reached, v_o actually becomes a fixed point, thereby destroying the integral control. The equation then reduces to the PWM PD linear controller form.

2) Performance Comparison With HM-Based SM Controllers: It should be noted that this controller is not of absolute robustness to line and load variations. Its robustness improves with switching frequency. Full robustness of any controller can only be achieved when the switching frequency is infinite. Now, considering that both line and load variations will affect the switching frequency and hence deteriorate the dc regulation in the conventional HM-based SM controlled converters [10], the adoption of the constant frequency PWM technique in SM controllers will provide comparatively better steady-state

[4]The derivation procedure of the control equations for the buck–boost converter is similar to that of the boost converter.

line and load regulated converters. On the other hand, the dynamic responses of the two controllers (assuming both types of controllers to operate at a similar averaged constant switching frequency) will not be differ significantly. Recall that in SM controlled systems, the dynamic behavior is mainly determined by the sliding coefficients. Apparently, if both types of controllers have the same set of sliding coefficients and are operating in the same frequency range, their dynamic responses will be similar.

3) Comparing the Proposed Approach to the Nonlinear PWM Controller Design Approach: It is also interesting to note that the derived controllers can be viewed as a type of nonlinear state-feedback controllers designed from nonlinear "per-cycle averaged models" of the converters. In fact, the method reported in [15] can be used to derive the same nonlinear duty cycle expression reported in this paper. The method used in nonlinear PWM controller design is to assume a large-signal average model of the converter at the start of the derivation [15]. In our approach, the model of the converter is retained in its discrete state-space form throughout the derivation. When the duty cycle is equivalent to the equivalent control, i.e., $d = u_{\rm eq}$, an averaging process takes place. Note that $u_{\rm eq}$ describes the *instantaneous* control required for SM control operation to occur. Hence, when the duty cycle control is employed to implement the $u_{\rm eq}$ over a finite time period of a switching cycle, the required instantaneity is spread over a switching cycle. Therefore, this can be considered as "per-cycle averaging" of the converter model. Thus, the main difference of our approach from that of nonlinear PWM control is that while the same assumption of an "average model" holds, our approach, which only averages the model during the implementation of the controller, retains much of the power converter dynamics. This results in a set of design restrictions: the existence conditions, which are evolved from the instantaneous dynamics of the converter, as required by the SM control theory. Such design restrictions are absent from the nonlinear PWM controller design approach. Finally, knowing that the abidance of the existence condition implies that the system's trajectory will strictly follow the desired sliding surface, the system's dynamic response will strictly obey the designed dynamics. Such stringency is not present in the nonlinear PWM controller design approach.

4) Design Constraints of the Proposed Voltage Controller: The ability to stabilize and control converter systems with right-half-plane-zero (RHPZ) characteristic in their duty-cycle-to-output-voltage transfer functions using the voltage mode controller comes at the expense of a lower bandwidth than the current mode controllers. This is also true for SM types of voltage controllers. The adoption of the PWM-based SM voltage controller does not change the fact that such frequency limitation exists. Lower values of sliding coefficients, i.e., controller bandwidth, are to be chosen for the PWM-based SM voltage controller for converters with RHPZ, as compared to the current mode controller. This explains why the best achievable response by the PWM-based SMVC boost converter is slower than the response obtainable from the peak current mode controlled boost converter (as illustrated later in the experimental results). Worthmentioning is that the restriction of the control parameter selection due to the RHPZ of the boost converter is actually inherently embedded in the existence conditions. The constraint of the condition automatically compromises for the system's RHPZ and prevents a high bandwidth to be selected.

D. Other Design Considerations

Briefly, the design of the PWM-based SM controller can be summarized as follows: selection of the desired settling time of the response and the type and amount of damping required; calculation of the corresponding sliding coefficients using the corresponding sets of equations, i.e., (19) and (20); inspection of the sliding coefficients's appropriateness using the existence conditions in Table II; and formulation of the control equations by substituting the selected sliding coefficients to calculate for K_{p1} and K_{p2}. The following addresses the issues concerning the implementation of the controller.

1) Bandwidth of Ramp Voltage Generator: The formulation of the ramp voltage signals is dependent on the instantaneous input and/or output voltages (see Table III). A change in load affecting the output voltage or a change in input voltage will both affect the ramp voltage. Hence, to ensure the correct generation of the ramp voltage signal corresponding to the dynamical behavior of input and/or output voltages, the bandwidth of the ramp voltage generator must be greater than the bandwidths of the input and/or output voltage variations. Note that this varying of the peak magnitude of the ramp signal with the input and/or output voltages is part of the controller's effort to maintain respectively the line and load regulation properties of the system.

2) Load Resistance Dependence: A close inspection of the control equations reveals that the control signal v_c is actually load dependent. Thus, for the controller to have good regulation performance against load changes, the instantaneous value of r_L should be fed back. However, this would require additional sensors and cumbersome computations, which complicate the controller. On the other hand, the dependence and sensitivity of v_c on the load can be minimized by a proper design of sliding coefficient such that $(\alpha_1)/(\alpha_2) \gg (1)/(r_L C)$. In such circumstance, the design value of load resistance can be made a constant parameter $R_{L(\rm nom)}$. If this is adopted, the real system's dynamics at SM operation will be changed from being ideal

$$\frac{d^2x_1}{dt^2} + \frac{\alpha_1}{\alpha_2} \cdot \frac{dx_1}{dt} + \frac{\alpha_3}{\alpha_2} \cdot x_1 = 0 \tag{30}$$

to the actual case of

$$\frac{d^2x_1}{dt^2} + \left(\frac{\alpha_1}{\alpha_2} + \frac{1}{r_L(t)C} - \frac{1}{R_{L(\rm nom)}(t)C}\right) \cdot \frac{dx_1}{dt} + \frac{\alpha_3}{\alpha_2} \cdot x_1 = 0 \tag{31}$$

where $r_L(t) \neq R_{L(\rm nom)}$ is the instantaneous load resistance, when the load differs the design value. However, since $(\alpha_1)/(\alpha_2) \gg (1)/(r_L C)$, the dynamics of the actual case will be very close to the ideal case.

3) Maximum Duty Cycle: Recalling that the boost and buck–boost type converters cannot operate with a switching signal u that has a duty cycle $d = 1$, a small protective device is

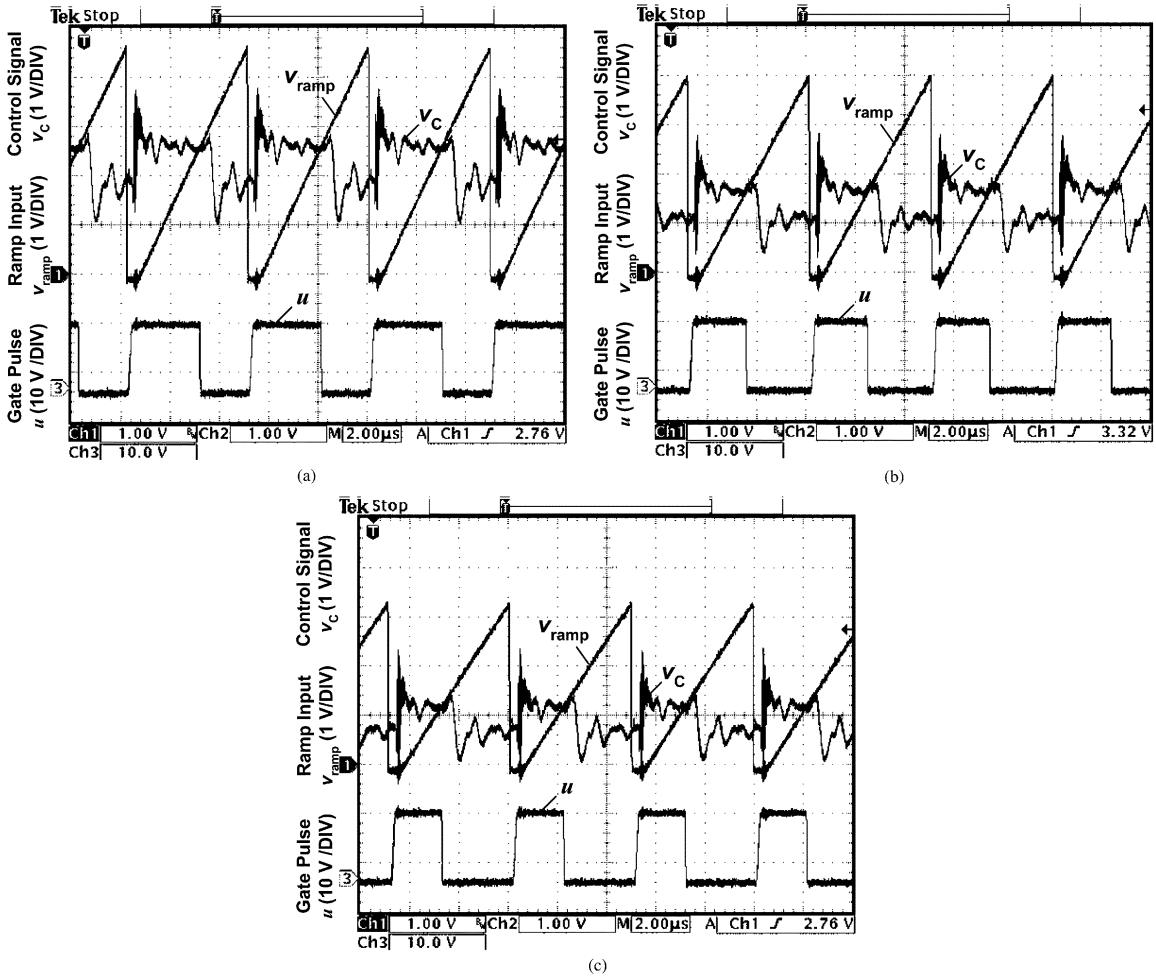

Fig. 4. Steady-state waveforms of control signal v_c, input ramp $v_{\rm ramp}$, and generated gate pulse u for the SMVC boost converter operating at full-load resistance $r_L = 24\ \Omega$. (a) $v_i = 20$ V. (b) $v_i = 24$ V, (a) $v_i = 28$ V.

TABLE IV
SPECIFICATION OF BOOST CONVERTER

Description	Parameter	Nominal Value
Input voltage	$v_{\rm i}$	24 V
Capacitance	C	230 μF
Capacitor ESR	c_r	69 mΩ
Inductance	L	300 μH
Inductor resistance	l_r	0.14 Ω
Switching frequency	$f_{\rm S}$	200 kHz
Minimum load resistance (full load)	$r_{\rm L(min)}$	24 Ω
Maximum load resistance (ten-percent load)	$r_{\rm L(max)}$	240 Ω
Desired output voltage	$V_{\rm od}$	48 V

required to ensure that the duty cycle of the controller's output is always $d < 1$.

III. EXPERIMENTAL RESULTS AND DISCUSSIONS

The derived PWM-based SM voltage controller has been experimentally verified on a buck converter [11]. In this section, we present the experimental verification of the PWM-based SMVC boost converter.

Table IV shows the specification of the 100 W boost converter used in this section. The PWM-based SM controller is designed to give an under-damped response at a bandwidth of $\omega_n = 1.25$krad/s, i.e., $\tau = 0.8$ ms, and $T_s = 4.0$ ms, and with damping coefficient $\zeta = 0.2$. From (19) and (20), the

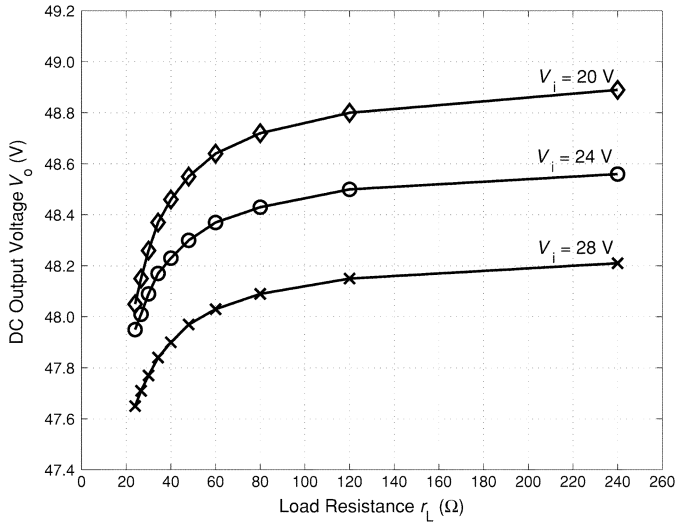

Fig. 5. Plots of dc output voltage V_o against load resistance r_L for the PWM-based SMVC boost converter at minimum, nominal, and maximum input voltages.

TABLE V
LOAD REGULATION PROPERTY FOR MINIMUM TO MAXIMUM LOAD. OUTPUT VOLTAGE AT NOMINAL OPERATING CONDITION $v_i = 24$ V AND $r_L = 24\ \Omega$ IS $v_{o(\text{nominal condition})} = 47.95$ V

Input Voltage	Voltage Deviation: $\Delta v_o = v_{o(240\ \Omega)} - v_{o(24\ \Omega)}$	Percentage Change: $\frac{\Delta v_o}{v_{o(\text{nominal condition})}}$ x 100 %
v_i= 20 V	0.84 V	1.75 % of $v_{o(\text{nominal condition})}$
v_i= 24 V	0.61 V	1.27 % of $v_{o(\text{nominal condition})}$
v_i= 28 V	0.56 V	1.16 % of $v_{o(\text{nominal condition})}$

TABLE VI
LINE REGULATION PROPERTY FOR MINIMUM TO MAXIMUM INPUT VOLTAGES. OUTPUT VOLTAGE AT NOMINAL OPERATING CONDITION $v_i = 24$ V AND $r_L = 24\ \Omega$ IS $v_{o(\text{nominal condition})} = 47.95$ V

Loading Condition	Voltage Deviation: $\Delta v_o = v_{o(v_i=20\ \text{V})} - v_{o(v_i=28\ \text{V})}$	Percentage Change: $\frac{\Delta v_o}{v_{o(\text{nominal condition})}}$ x 100 %
Minimum load (240 Ω)	0.68 V	1.42 % of $v_{o(\text{nominal condition})}$
Half load (48 Ω)	0.58 V	1.21 % of $v_{o(\text{nominal condition})}$
Full load (24 Ω)	0.40 V	0.83 % of $v_{o(\text{nominal condition})}$

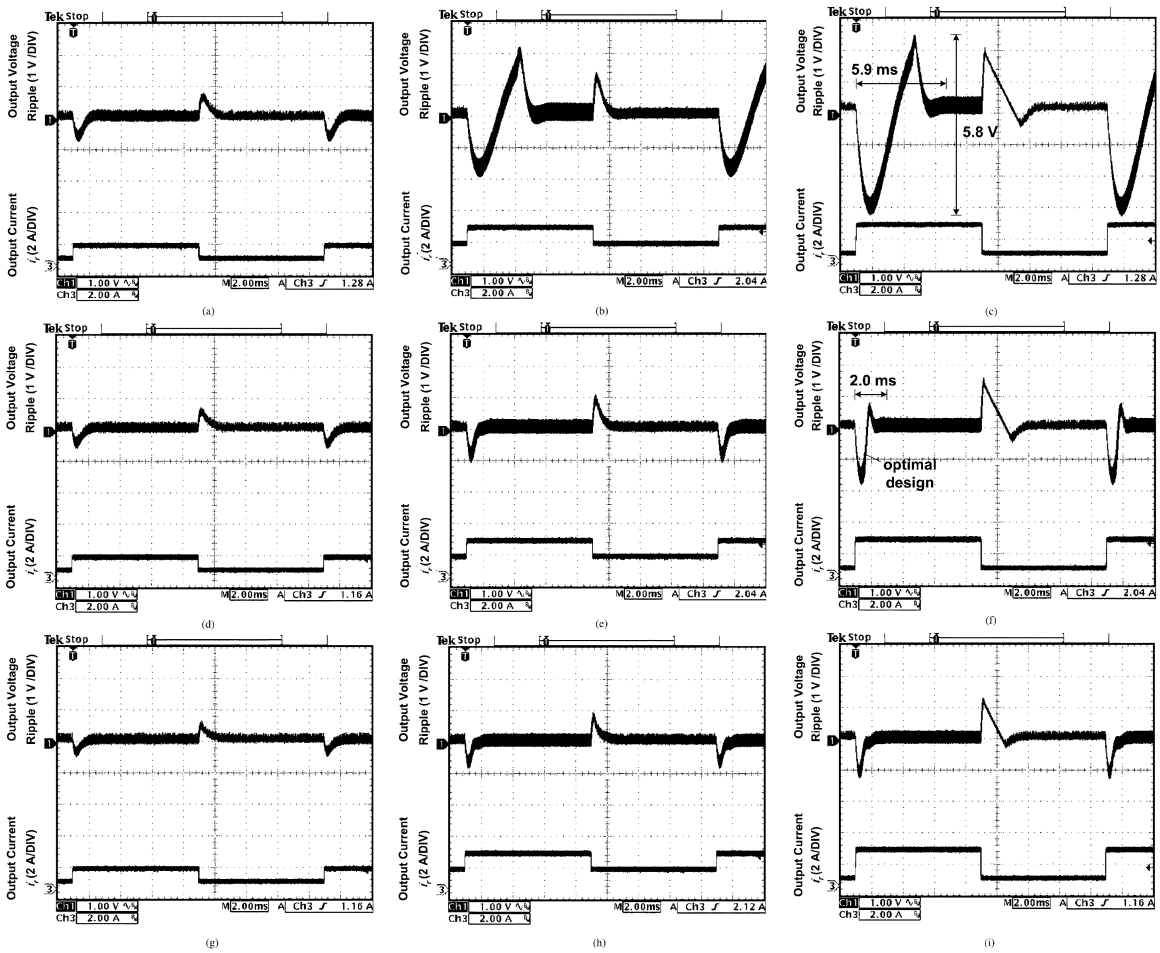

Fig. 6. Experimental waveforms of output voltage ripple $\tilde{v_o}$ and output current i_r of the boost converter with the peak current mode controller operating at input voltage 20 V (minimum), 24 V (nominal), and 28 V (maximum), and alternating between load resistances 24 Ω (minimum), 48 Ω (half), and 240 Ω (maximum). (a) $v_i = 20$ V (0.2/1.0 A). (b) $v_i = 20$ V (1.0/2.0 A). (c) $v_i = 20$ V (0.2/2.0 A). (d) $v_i = 24$ V (0.2/1.0 A). (e) $v_i = 24$ V (1.0/2.0 A). (f) $v_i = 24$ V (0.2/2.0 A). (g) $v_i = 28$ V (0.2/1.0 A). (h) $v_i = 28$ V (1.0/2.0 A). (i) $v_i = 28$ V (0.2/2.0 A).

sliding coefficients are determined as $(\alpha_1)/(\alpha_2) = 2500$ and $(\alpha_3)/(\alpha_2) = 39130435$. Note that designing for the full-load condition, $(\alpha_1)/(\alpha_2) \gg (1)/(r_{L(\min)}C)$, i.e., $2500 \gg 181.1$. Setting the reference voltage in the controller as $V_{\text{ref}} = 8$ V, the feedback divider ratio can be calculated as $\beta = (V_{\text{ref}}/V_{\text{od}}) = (1/6)$. Finally, control parameters are determined as $K_{p1} = \beta L((\alpha_1)/(\alpha_2) - (1)/(r_L C)) = 0.12$ and $K_{p2} = (\alpha_3)/(\alpha_2)LC = 2.7$.

A. Variable Ramp

Fig. 4(a)–(c) shows the steady-state waveforms of the SM controller for the boost converter with minimum, nominal, and

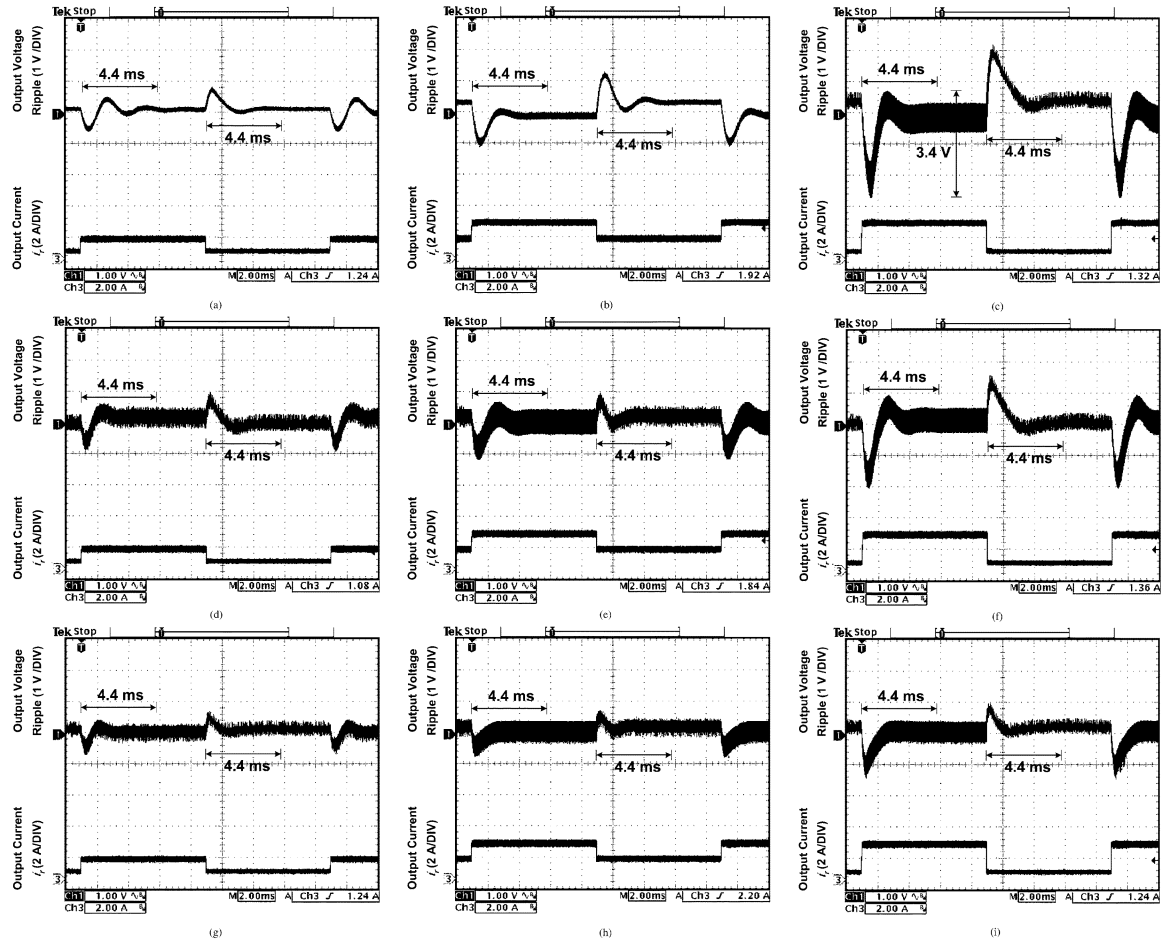

Fig. 7. Experimental waveforms of output voltage ripple $\widetilde{v_o}$ and output current i_r of the boost converter with the 1.5 krad/s bandwidth PWM-based SM controller operating at input voltage 20 (minimum), 24 (nominal), and 28 V (maximum), and alternating between load resistance 24 Ω (minimum), 48 Ω (half), and 240 Ω (maximum). (a) $v_i = 20$ V (0.2/1.0 A). (b) $v_i = 20$ V (1.0/2.0 A). (c) $v_i = 20$ V (0.2/2.0 A). (d) $v_i = 24$ V (0.2/1.0 A). (e) $v_i = 24$ V (1.0/2.0 A). (f) $v_i = 24$ V (0.2/2.0 A). (g) $v_i = 28$ V (0.2/1.0 A). (h) $v_i = 28$ V (1.0/2.0 A). (i) $v_i = 28$ V (0.2/2.0 A).

maximum input voltages. The control signal v_c is formulated through analog computation of the feedback signals v_o, v_i, and i_c using the expression described in (28). The ramp signal v_{ramp} is generated with peak magnitude as described in (29) using feedback signals v_o, v_i through an analog variable ramp generator. Both v_c and v_{ramp} are fed into a pulsewidth modulator to generate the gate pulse u, for the switching of the boost converter. Clearly, the figures show the different ramp magnitudes and the duty ratios for different input voltages. Specifically, at $v_i = 20$ V, 24 V, and 28 V, the magnitudes of v_{ramp} are roughly 4.67, 4.0, and 3.33 V, respectively, and the duty ratio d are roughly 0.56, 0.48, and 0.44, respectively.

B. Regulation Performance

Fig. 5 shows the measured dc output voltage versus the operating load resistance for three input voltage conditions, i.e., minimum, nominal, and maximum input voltages.A tabulation of the data in terms of the load and line regulation properties is also given in Tables V and VI respectively. According to Table V, the maximum load-regulation error occurs at $v_i = 20$ V, with a deviation of 1.75% from $v_{o(\text{nominal condition})}$. Similarly, it can be found from Table VI that the maximum line-regulation error occurs at minimum load $r_L = 240\ \Omega$, with a deviation of 1.42% from $v_{o(\text{nominal condition})}$.

C. Performance Comparison With Peak Current Mode Controller

The dynamic behavior of the PWM-based controller is compared to that of a UC3843 peak current mode PWM controller that is optimally tuned to operate at the step load change from $r_L = 240\ \Omega$ to $r_L = 24\ \Omega$ for the input condition $v_i = 24$ V. Fig. 6(a)–(i) shows the experimental waveforms of the peak current mode controlled boost converter operating at a load resistance that alternates between $r_L = 24\ \Omega$ and $r_L = 240\ \Omega$ for various input voltages.

It can be seen that with the peak current mode PWM controller, the dynamic behavior of the system differs for different operating conditions. Specifically, the response becomes less oscillatory at higher input voltages. Moreover, the dynamic behavior and transient settling time are also different between the various cases of operating conditions. Specifically, at a lower step current change, i.e., 0.2 A to 1.0 A, the response of the system becomes critically damped, instead of its optimally designed response which is slightly under-damped, as shown in

Fig. 6(f). Furthermore, in the worst case operating condition: $v_i = 20$ V and step output current change of 0.2 to 2.0 A, the system has a settling time of 5.8 ms and a relatively high voltage ripple swing of 5.6 V [see Fig. 6(c)], which is much deviated from the optimally designed value of 2 ms and a voltage ripple swing of 2.6 V [see Fig. 6(f)]. This is expected since the peak current-mode controller is designed under a linearized small signal model that is only optimal for a specific operating condition. Thus, when a different operating condition is engaged, the responses varies.

On the other hand, with the PWM-based SM controller, the dynamic behavior of output voltage ripple is basically similar (i.e., slightly under-damped) for all operating input and load conditions. This is illustrated in Fig. 7(a)–(i), which shows the experimental waveforms of the PWM-based SM controlled boost converter operating at the same set of operating conditions as the peak current mode controlled boost converter.

Furthermore, the transient settling time, which is around 4.4 ms, is also independent of the direction and magnitude of the step load change and the operating input voltages. This coincides with our design, which being a 1.25 krad/s bandwidth controller, is expected to have a settling time of $5\tau = (5/1.25) = 4.0$ ms. Moreover, in the worst case operating condition: $v_i = 20$ V and step output current change of 0.2 to 2.0 A, the settling time is still around 4.4 ms and the voltage ripple swing is 3.4 V [see Fig. 7(c)]. This is close to the optimally designed system, which has voltage ripple swing of 3.0 V [see Fig. 7(f)]. Hence, the strength of the SM controller in terms of robustness in the dynamic behavior under different operating conditions and uncertainties is demonstrated. Additionally, the example also illustrates a major difference between a large-signal controlled system (SM) and a small-signal controlled system (PWM), that is, the former complies to the design with a similar response for all operating conditions, while the response of the latter will only comply to the design at a specific operating condition.

IV. Conclusion

A unified approach to the design of fixed-frequency PWM-based SM controllers for all dc–dc converter types operating in continuous conduction mode is presented. For completeness sake, the design approach is concurrently illustrated on the buck, boost, and buck–boost converters. Simple control equations for implementation of the PWM-based SM voltage controllers for the different converters are also derived. An experimental prototype of the derived boost controller/converter system is developed to validate the design methodology. Different static and dynamic tests with line and load changes are also performed to test the functionalities of such systems. It can be concluded from the results that the PWM-based SM voltage controllers are feasible for common dc–dc conversion purposes.

Acknowledgment

The authors would like to thank C.-K. Wu for developing the experimental prototype.

References

[1] V. Utkin, J. Guldner, and J. X. Shi, *Sliding Mode Control in Electromechanical Systems*. London, U.K.: Taylor and Francis, 1999.
[2] H. W. Whittington, B. W. Flynn, and D. E. Macpherson, *Switched Mode Power Supplies: Design and Construction*, 2nd ed. New York: Wiley, 1997.
[3] B. J. Cardoso, A. F. Moreira, B. R. Menezes, and P. C. Cortizo, "Analysis of switching frequency reduction methods applied to sliding-mode controlled dc-dc converters," in *Proc. IEEE Appl. Power Electron. Conf. Expo. (APEC'92)*, Feb. 1992, pp. 403–410.
[4] P. Mattavelli, L. Rossetto, G. Spiazzi, and P. Tenti, "General-purpose sliding-mode controller for dc/dc converter applications," in *Rec. IEEE Electron. Specialists Conf. (PESC'93)*, Jun. 1993, pp. 609–615.
[5] V. M. Nguyen and C. Q. Lee, "Tracking control of buck converter using sliding-mode with adaptive hysteresis," in *Rec. IEEE Electron. Specialists Conf. (PESC'95)*, Jun. 1995, vol. 2, pp. 1086–1093.
[6] S. K. Mazumder and S. L. Kamisetty, "Experimental validation of a novel multiphase nonlinear VRM controller," in *Rec. IEEE Electron. Specialists Conf. (PESC'04)*, Jun. 2004, pp. 2114–2120.
[7] V. M. Nguyen and C. Q. Lee, "Indirect implementations of sliding-mode control law in buck-type converters," in *Proc. IEEE Appl. Power Electron. Conf. Expo. (APEC'96)*, Mar. 1996, vol. 1, pp. 111–115.
[8] J. Mahdavi, A. Emadi, and H. A. Toliyat, "Application of state-space averaging method to sliding-mode control of PWM DC/DC converters," in *Proc. IEEE Conf. Ind. Appl. (IAS'97)*, Oct. 1997, vol. 2, pp. 820–827.
[9] J. Mahdavi, M. R. Nasiri, A. Agah, and A. Emadi, "Application of neural networks and state-space averaging to a DC/DC PWM converter in sliding-mode operation," *IEEE/ASME Trans. Mechatron.*, vol. 10, no. 1, pp. 60–67, Feb. 2005.
[10] S. C. Tan, Y. M. Lai, M. K. H. Cheung, and C. K. Tse, "On the practical design of a sliding-mode voltage controlled buck converter," *IEEE Trans. Power Electron.*, vol. 20, no. 2, pp. 425–437, Mar. 2005.
[11] S. C. Tan, Y. M. Lai, C. K. Tse, and M. K. H. Cheung, "A fixed-frequency pulsewidth-modulation-based quasi-sliding-mode controller for buck converters," *IEEE Trans. Power Electron.*, vol. 20, no. 6, pp. 1379–1392, Nov. 2005.
[12] R. Venkataramanan, A. Sabanoivc, and S. Ćuk, "Sliding-mode control of dc-to-dc converters," in *Proc. IEEE Conf. Ind. Electron., Contr. Instrum. (IECON'85)*, 1985, pp. 251–258.
[13] H. Sira-Ramirez and M. Ilic, "A geometric approach to the feedback control of switch mode DC-to-DC power supplies," *IEEE Trans. Circuits Syst.*, vol. 35, no. 10, pp. 1291–1298, Oct. 1988.
[14] H. Sira-Ramirez, "A geometric approach to pulsewidth modulated control in nonlinear dynamical systems," *IEEE Trans. Autom. Contr.*, vol. 34, no. 3, pp. 184–187, Feb. 1989.
[15] L. Martinez, A. Poveda, J. Majo, L. Garcia-de-Vicuna, F. Guinjoan, J. C. Marpinard, and M. Valentin, "Lie algebras modeling of bidirectional switching converters," in *Proc. Eur. Conf. Circuit Theory Design (ECCTD'93)*, Sep. 1993, vol. 2, pp. 1425–1429.
[16] C. C. Wu and C. M. Young, "A new PWM control strategy for the buck converter," in *Proc. IEEE Conf. Ind. Electron. (IECON'99)*, 1999, pp. 157–162.
[17] J. Ackermann and V. Utkin, "Sliding-mode control design based on Ackermann's formula," *IEEE Trans. Autom. Contr.*, vol. 43, no. 2, pp. 234–237, Feb. 1998.
[18] P. Mattavelli, L. Rossetto, and G. Spiazzi, "Small-signal analysis of dc–dc converters with sliding-mode control," *IEEE Trans. Power Electron.*, vol. 12, no. 1, pp. 96–102, Jan. 1997.
[19] G. Spiazzi and P. Mattavelli, "Sliding-mode control of switched-mode power supplies," in *The Power Electronics Handbook*. Boca Raton, FL: CRC, 2002, ch. 8.
[20] H. Sira-Ramirez, "On the generalized PI sliding-mode control of dc-to-dc power converters: A tutorial," *Int. J. Contr.*, vol. 76, no. 9/10, pp. 1018–1033, 2003.

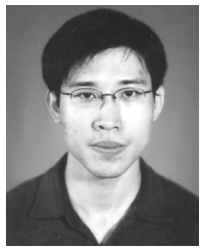

Siew-Chong Tan (S'00–M'06) received the B.Eng. (with honors) and M.Eng. degrees in electrical and computer engineering from the National University of Singapore, Singapore, in 2000 and 2002, respectively, and the Ph.D. degree from the Hong Kong Polytechnic University, Hong Kong, in 2005.

He worked briefly as a Research Associate and then a Post-Doctoral Fellow in the Department of Electronic and Information Engineering, Hong Kong Polytechnic University, where he is currently a Lecturer. His research interests include motor drives and power electronics.

Y. M. Lai (M'92) received the B.Eng. degree in electrical engineering from the University of Western Australia, Perth, WA, Australia, the M.Eng.Sc. degree in electrical engineering from University of Sydney, Sydney, Australia, and the Ph.D. degree from Brunel University, London, U.K., in 1983, 1986, and 1997, respectively.

He is an Assistant Professor with Hong Kong Polytechnic University, Hong Kong, and his research interests include computer-aided design of power electronics and nonlinear dynamics.

Chi K. Tse (M'90–SM'97–F'06) received the B.Eng. degree with first class honors and the Ph.D. degree from the University of Melbourne, Melbourne, Australia, in 1987 and 1991, respectively.

He is presently Chair Professor and Head of Department of Electronic and Information Engineering at the Hong Kong Polytechnic University, Hong Kong. His research interests include chaotic dynamics, power electronics and chaos-based communications. He is the author of the books *Linear Circuit Analysis* (Addison-Wesley, 1998) and *Complex Behavior of Switching Power Converters* CRC Press, 2003), coauthor of *Chaos-Based Digital Communication Systems* (Springer-Verlag, 2003) and *Reconstruction of Chaotic Signals with Applications to Chaos-Based Communications* (TUP, 2005), and co-holder of a U.S. patent and two other pending patents.

Dr. Tse received the Best Paper Award from IEEE TRANSACTIONS ON POWER ELECTRONICS in 2001, Dynamics Days Europe Presentation Prize in 2002, and the Best Paper Award from *International Journal of Circuit Theory and Applications* in 2003. In 2005, he was named an IEEE Distinguished Lecturer. Dr. Tse was an Associate Editor of the IEEE TRANSACTIONS ON CIRCUITS AND SYSTEMS—I: FUNDAMENTAL THEORY AND APPLICATIONS from 1999 to 2001, and since 1999, has been an Associate Editor of the IEEE TRANS. POWER ELECTRON.. He also served as Guest Editor of theIEEE TRANSACTIONS ON CIRCUITS AND SYSTEMS—I: FUNDAMENTAL THEORY AND APPLICATIONS in 2003, and of *Circuits, Systems and Signal Processing* in 2005. He currently also serves as an Associate Editor for the *International Journal of Systems Science*.